Determination of the Fermi Surface of Molybdenum Using the de Haas–van Alphen Effect

J. A. Hoekstra* and J. L. Stanford
Ames Laboratory-USAEC and Department of Physics, Iowa State University, Ames, Iowa 50010
(Received 26 December 1972)

The de Haas–van Alphen effect in molybdenum has been studied in detail using large impulsive magnetic fields. Digital data recording, fast Fourier-frequency analysis by computer, and dynamic calibration of the entire apparatus have been used to obtain the de Haas–van Alphen frequencies to a high degree of accuracy. Several new frequency branches associated with the electron-jack piece of the Fermi surface are reported. Frequency branches exhibiting high angular accuracy and resolution are reported for all branches that have previously been detected by other de Haas–van Alphen investigators. A quantitative description of all sheets of the Fermi surface is presented, along with comparisons with other Fermi-surface radii obtained by use of the radio-frequency-size-effect (RFSE) technique. The Mueller inversion technique for obtaining Fermi-surface radii from the de Haas–van Alphen area data was used whenever possible. The de Haas–van Alphen results presented are consistent with an estimate of 2.5% of the ΓH dimension for the size of the gap between the jack and the octahedral Fermi-surface pieces. Thus the question about the size of this gap as raised by discrepancies greater than the combined experimental errors existing in current RFSE data is resolved. The spin-orbit parameter is not found to be anomalously higher than that for tungsten.

I. INTRODUCTION

The Fermi surface (FS) and the electronic structure of molybdenum have been the subjects of several extensive investigations over the past few years. Most of the results have been interpreted in terms of revisions of a model for the chromium-group metals (Cr, Mo, W) first proposed by Lomer,[1] who used the energy bands for Fe as calculated by Wood.[2] The initial model was later corrected for the particular case of molybdenum.[3] Theoretical augmented-plane-wave (APW) calculations for Mo done by Loucks[4] exhibit qualitative agreement with the Lomer model, but the quantitative results are subject to numerical errors due to an incorrect size for the unit cell used in determining the potential applied in the calculation.[5]

On the experimental side, studies have been made of the magnetoresistance,[6–8] anomalous skin effect,[9] magnetoacoustic effect,[10,11] cyclotron resonance,[12] and the de Haas–van Alphen (dHvA) effect.[13–16]

The recent radio-frequency-size-effect (RFSE) measurements of Boiko, Gasparov, and Gverdtsiteli[17] and Cleveland and Stanford[18] provide many caliper dimensions of the FS but the data presented in these two investigations differ by 6%, a discrepancy which is greater than the combined experimental errors claimed by the investigators. The RFSE data are most helpful in defining the shapes of the larger FS pieces, but are hard to obtain and interpret for the ellipsoids and lenses, where the RFSE signals lie close together in magnetic field value, and are difficult to separate and follow as a function of angle. The separation or gap between the jack and the octahedral FS pieces was estimated by Boiko *et al.* as 2.5% of the ΓH dimension, while Cleveland and Stanford's estimate for the gap was 7%. The larger gap was explained by choosing a value of the spin-orbit parameter for Mo larger than that predicted by Mattheiss[19] for W. The effects of spin-orbit coupling should be more pronounced in W, where the gap is 5%,[20] than in Mo.

This investigation of Mo was undertaken to provide complete and accurate data concerning the extremal areas associated with each of the pieces of the FS using the pulsed-field dHvA technique. The data were used to obtain the FS radii and thus clarify the discrepancy existing in the current RFSE data, and to resolve the question about the size of the gap between the jack and the octahedron caused by the spin-orbit interaction.

II. EXPERIMENTAL PROCEDURE

The impulsive-field apparatus and data reduction techniques used were essentially the same as those reported by Girvan *et al.*[20] The experimental details are given in a previous report,[21] so only an improvement in the frequency-analysis method will be discussed in this paper.

The single-crystal samples used in this investigation were spark cut from the same single-crystal rod of Mo from which Cleveland obtained samples for his RFSE esperiment.[22] The rod, purchased from Westinghouse Lamp Division, has a residual resistance ratio ($R_{300\ K}/R_{4.2\ K}$) of 5000 as determined by use of the eddy-current-decay method.[23] Two samples for this investigation were cut in the form of long thin square bars—one with a ⟨100⟩ crystallographic axis parallel to the length of the bar and the other with a ⟨110⟩ direction as the long axis. These samples were electropolished to a diameter of 0.5 mm and a length of 5 mm, using a 6% solution

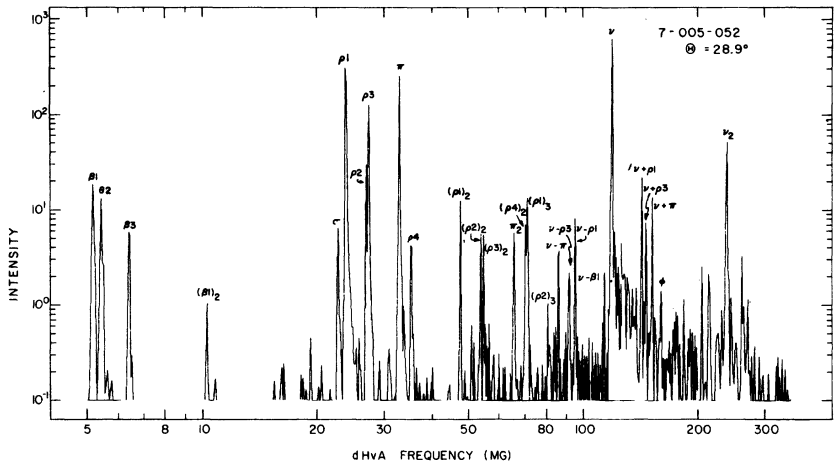

FIG. 1. Fast Fourier-frequency analysis of one set of dHvA data. The fundamental frequencies from this analysis are plotted and labeled in Fig. 2 at 28.9° from [010] in the (001) plane.

of perchloric acid in methanol cooled with a mixture of dry ice and acetone.

A sample was mounted in a pickup coil housed in the drive wheel of the sample holder.[24] The drive-wheel assembly was detached from the drive-shaft assembly and mounted in a jig capable of keeping the plane of rotation of the drive wheel parallel to a Polaroid x-ray camera used for checking the orientation of the sample. The x-ray beam, entering a small hole in the wheel parallel to its axle, struck the tip of the sample which slightly protruded out of the end of the pickup coil. The Laue back-reflection diffraction pattern obtained permitted determination of the plane of rotation of the sample to within 1° of a chosen crystallographic direction.

To obtain all of the frequency data possible from the sample, one would like to have some way of being able to discriminate against some frequencies while enhancing others. Then a higher-amplitude signal from a given set of frequencies would enable a more accurate determination of the frequencies involved. One data run for each orientation plane with a given sample was made at a temperature of 4.2 K using a peak field of 90 kG. This mode of operation enhanced the amplitudes of frequencies arising from the lenses and the ellipsoids. A second data run for each plane and sample was made at 1.2 K using a peak field of 170 kG. At this temperature and higher field the frequencies associated with the larger and/or higher-effective-mass orbits arising from the electron jack and the hole octahedron were brought out.

All of the results reported here were obtained with the aid of the high-speed digital recording equipment developed by Panousis.[25]

The frequency-analysis program[21] used the fast Fourier subroutine RHARM from the IBM scientific subroutine package. This analysis is 10–60 times faster than the filter-periodogram technique described by Panousis[24] with comparable frequency accuracy and resolution. Figure 1 shows a fast Fourier-frequency analysis of dHvA data taken at 28.9° from [010] in the (001) plane. The graph is a composite of several small-range frequency scans, since the program works best on frequency scans of one octave or less. The frequency results shown were obtained with about 45 sec of CPU time, while the time used to obtain very similar filter-periodogram frequency results for the data set was around 35 min of CPU time on an IBM 360/65 computer. The peaks labeled $\beta 1$, $\beta 2$, $\beta 3$ are plotted as points labeled β for frequencies at 28.9° from [010] in the (001) plane as shown in Fig. 2, a semilogarithmic plot of all of the data obtained in the (001) and $(1\bar{1}0)$ planes. Peaks labeled with subscripts in Fig. 1 [such as $(\beta 1)_2$] are second harmonics, and peaks with two frequencies (such as $\gamma \pm \pi$) are sums and differences of the appropriate fundamental terms. Only frequencies identified as fundamental were plotted in Fig. 2. The 27 peaks identified in Fig. 1 illustrate the power of the analysis program to extract many frequencies with high accuracy and resolution from a single data set.

The amplifiers in the apparatus were capable of passing time frequencies in only a certain given range (~5–100 kHz), and the dHvA digital equipment was capable of taking data at equal time intervals of 4 μsec minimum (i.e., only two points per cycle were obtained for a 125 kHz signal). Since dHvA oscillations are periodic in $1/H$ rather than in real time, for a given pair of data points there are minimum and maximum values for possible dHvA frequencies contained in the data, as given by the relation

$$F_t = \left| \frac{\Delta(1/H)}{\Delta t} \right| F_{\mathrm{dHvA}} ,$$

where Δt and $\Delta(1/H)$ are computed from this pair of points, the time frequency F_t is one of the amplifier frequency limits and the corresponding dHvA frequency limit is F_{dHvA}. The upper amplifier limit

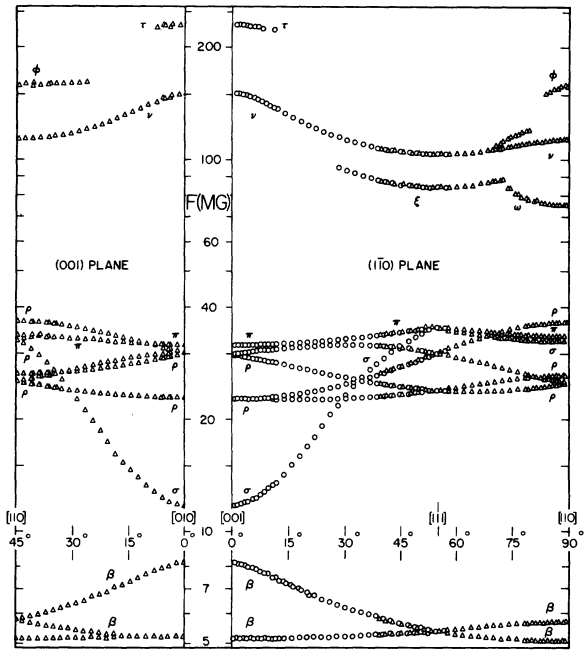

FIG. 2. Variations of the fundamental dHvA frequencies in molybdenum for field directions in the (001) and (1$\bar{1}$0) planes. The geometric axes for the rod-shaped samples are Δ, [110] and O, [001].

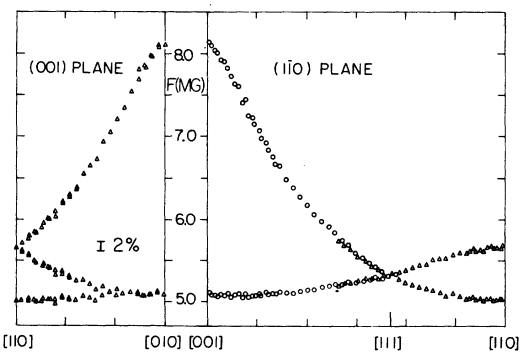

FIG. 3. Linear plot of low-frequency dHvA data for field directions in the (001) and (1$\bar{1}$0) planes.

assures the taking of data at a rate of more than two points per cycle. The best analysis is obtained when data is analyzed for a given dHvA frequency using only those data points which lie within the time frequency limitations given above. A time constant of 40 μsec was found appropriate to correct for the time delay introduced by the finite inductance of the "noninductive" standard resistor, for eddy-current effects, and for other effects, including electronics, capable of introducing a time delay.[25] This correction produced dHvA frequencies that were the same for both rising-field and falling-field data. Corresponding frequencies from each of the four data sets obtained at a given angle were averaged together to produce a single value which could be plotted on graphs of the data.

The pulse solenoid was calibrated using the dHvA effect itself to make a dynamic calibration of the entire apparatus. The [111] frequency of the ν oscillation in tungsten, determined by O'Sullivan and Schirber[26] to be 98.8 ± 0.2 MG with the aid of NMR measurements of quasistatic fields, was used as the frequency standard.

The experimental data which are presented in Sec. III were subjected to the following criteria: (i) The frequency presented should be the average of corresponding frequencies found in the four data sets taken at that angle. (ii) The frequency should be a member of a set of frequencies which are smoothly varying in value and amplitude as a function of angle of observation. (iii) Sets of frequencies which can be identified as second or third harmonics or sums and differences of other reported frequencies are omitted.

III. FREQUENCY RESULTS

The angular dependence of the fundamental dHvA frequencies corresponding to extremal cross-sectional areas of the FS of Mo are shown in Figs. 2–7. In all of these figures the symbol Δ is used to represent data taken with the [110] sample while the symbol O is used for the [001] sample. The labels for the frequency branches are those used by Girvan *et al.*,[20] except for the β used for lens frequencies, which do not exist in W. A drawing of a model FS for W, whose FS is similar to that for Mo, is shown in Fig. 8. Differences between the Fermi surface of Mo and W are discussed in Sec. IVA. The nomenclature for the various FS pieces is due to Sparlin and Marcus.[15] Γ, N, H, P, and Δ are standard labels for symmetry points in the Brillouin zone for Mo.

The only correction applied to all of the data was that for angle calibration.[21] Although the approxi-

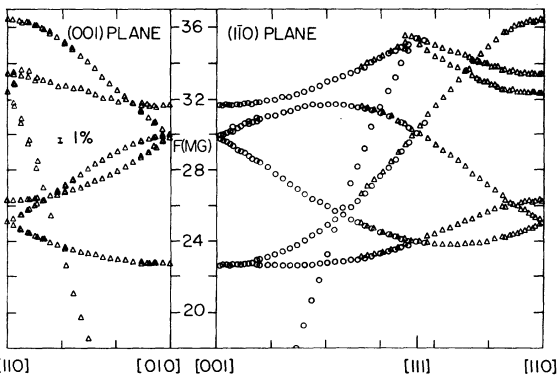

FIG. 4. Linear plot of medium-frequency dHvA data for field directions in the (001) and (1$\bar{1}$0) planes.

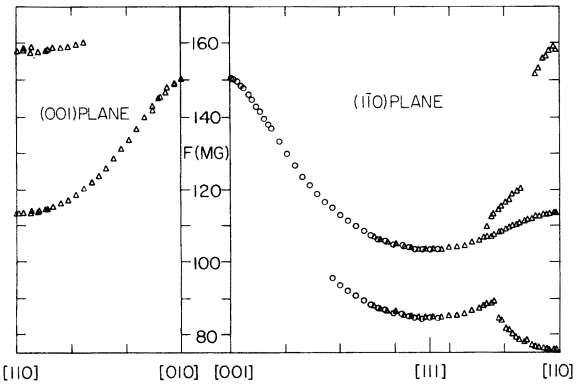

FIG. 5. Linear plot of high-frequency dHvA data for field directions in the (001) and (1$\bar{1}$0) planes.

mate symmetry direction of the sample for a certain sample-holder angle setting was known and used to determine the angular interval over which the data were taken, the final choice of the symmetry direction was made from the symmetry of the plotted frequency information about some particular angle. In Figs. 2–5 a symmetry direction was chosen for the corrected data taken over an approximately 60° range with a given sample and plane of orientation. A density of data as a function of angle greater than one set of frequencies per approximate 2° interval indicates the data were folded about the chosen symmetry direction. dHvA frequencies measured at a given symmetry direction should be identical, no matter which plane of orientation containing that

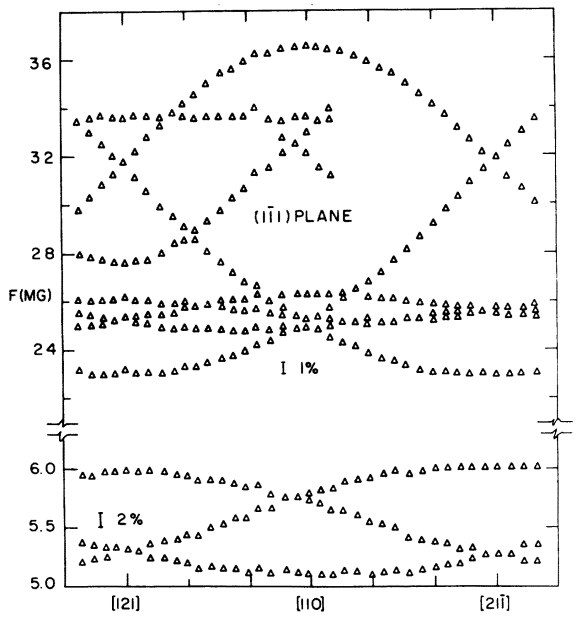

FIG. 6. Linear plot of low- and medium-frequency dHvA data for field directions in the (1$\bar{1}$1) plane. Note the break in scale for F (MG).

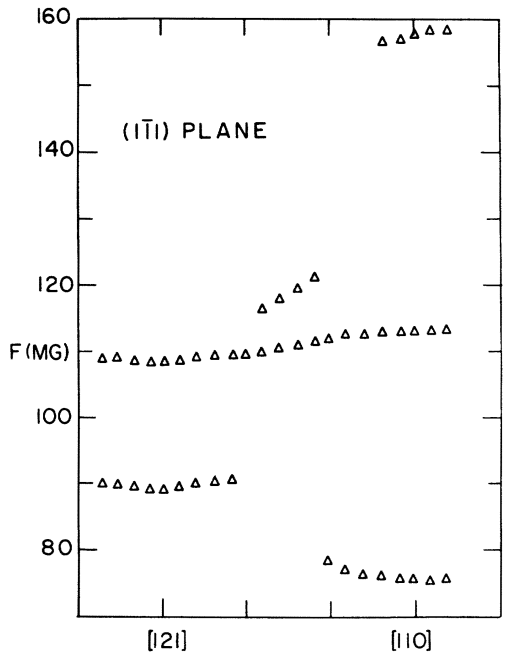

FIG. 7. Linear plot of high-frequency dHvA for field directions in the (1$\bar{1}$1) plane.

direction is chosen or which sample is being used. These frequencies, listed in Table I along with values determined by other experimentalists, can be compared for a given symmetry direction. Any discrepancies found are the result of misalignment of the sample in the plane of rotation, or the precision with which a given frequency can be determined (usually better than $\frac{1}{2}$%, except for around 1% for low frequencies).

Figures 3–5 are linear plots for the (001) and (1$\bar{1}$0) planes of most of the data appearing in Fig. 2, a semilogarithmic plot. The precision with which the samples were oriented can be seen from several aspects of these data. The folded data show very little scatter as a function of angle near the [110] and [001] symmetry directions. The scatter in the folded data at [010] in the (001) plane is a function entirely of the choice of a symmetry direction at [110], since all of the information reported in the plane came from the [110] sample. The scatter in the data appearing near [111] in the (1$\bar{1}$0) plane, where the data came from both samples, is a measure of the ability (a) to place each of the two samples in the (1$\bar{1}$0) plane, (b) to apply the same angle correction for a given dial reading on the sample holder, and (c) to pick a symmetry direction for the folded data at 0° and 90°. Once these three things have been done, there are no additional variables to be adjusted to make the data from these two samples to better overlap.

In Fig. 2 the frequency branches labeled β arise

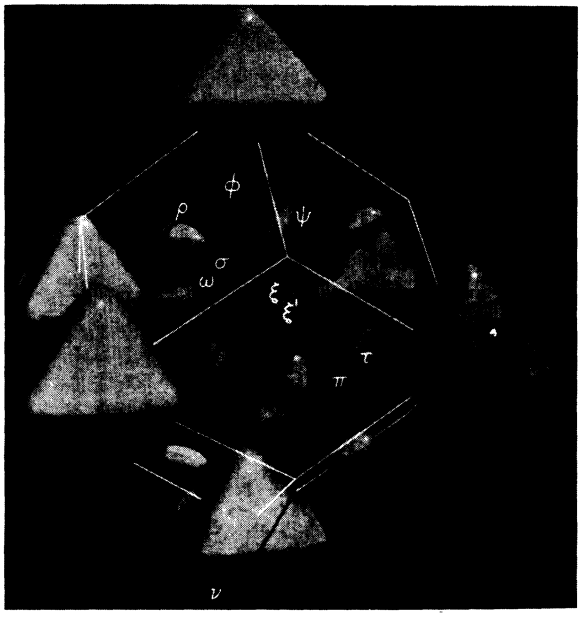

FIG. 8. Drawing of a model FS for tungsten, whose FS is similar to that for molybdenum. Some extremal orbits expected to give rise to a dHvA effect are shown as black lines. The Brillouin zone is indicated by white lines. Differences between the FS of molybdenum and tungsten are discussed in Sec. IV A. Figure reproduced from Ref. 20.

from orbits around the 6 electron lenses situated at each of the symmetry points Δ in the Brillouin zone. The ρ branches arise from the orbits associated with the 12 ellipsoids situated at the symmetry points N. The single frequency branch ν comes from orbits around the 6 equivalent octahedra located at the points H.

The rest of the orbits can be identified with the electron jack at Γ in the center of the zone, as shown in Fig. 8. The frequency branches π and σ correspond to orbits around the balls and necks, respectively. The τ frequency branch arises from a central orbit around four balls of the jack. The ω frequency branch, due to a noncentral orbit containing part of two adjacent balls and the body between them, is shown in the $(1\bar{1}0)$ plane in Figs. 2 and 5 and should also appear in the (001) plane at [110] and exhibit some angular dependence. Although this frequency branch probably existed in the raw data, it could not be sorted out from the pattern of second and third harmonics arising from data in the 25–40-MG range, and was therefore omitted. The two data points between 71° and 73°, which look as if they could be part of the ξ frequency branch, actually belong to the end of the ω frequency branch, as determined by comparison of their amplitudes with those of nearby data points in the two branches. The unlabeled frequency branch which appears at angles between the ξ and φ frequency branches can be explained as arising from a noncentral orbit probably encompassing the body and one ball of the jack as an intermediate between the ξ frequencies coming from orbits around the body of the jack, and the φ frequencies coming from an orbit encompassing two of the balls and the body between them.

Data for the $(1\bar{1}1)$ plane are shown in linear plots in Figs. 6 and 7. Note the break in the frequency scale in Fig. 6. The right half of this figure is missing some data because data were taken over a shorter angular range at high field for this plane. The angular scale shown with tick marks every 10° was that used in determining a symmetry direction for three frequency branches chosen for use in inversion of ellipsoid and octahedron data (see Sec. IV). It is obvious that these data do not have the symmetry which they should, and therefore, the data have not been folded about the symmetry direction. However, this plane is extremely sensitive to small misalignments of the sample. If the sample is only 1° out of the $(1\bar{1}1)$ plane, the four frequencies which should all cross at 25.1 MG at exactly [110] will not cross there, but will be shifted. The new crossing point for those frequency branches lying entirely between 24 and 27 MG in this plane can be greater than 10° from [110]. These three frequency branches in the data exhibit the most deviation from the expected symmetry pattern. Notice also the 2° uncertainty in the exact position for the [110] direction. A second attempt to orient the sample in this plane resulted in data almost identical to that presented here. It is estimated that an alignment error of less than 1° can account for the symmetry problems shown by this plane, and this fact is used along with the successful overlay of the data in the other two orientation planes to determine the uncertainty of the plane of orientation of a sample with respect to the magnetic field as 1° or less.

IV. DISCUSSION OF THE RESULTS

A. General Considerations

The experimental information about the FS of a metal obtained through the detection of the dHvA frequencies is in terms of extremal cross-sectional areas $A_0(E_F)$ of the FS normal to the applied magnetic field. The frequency F for these dHvA oscillations is given by the usual Onsager-Lifshitz-Kosevich equation

$$F=\frac{c\hbar}{2\pi e}A_0(E_F)=104.7\left(\frac{\mathrm{MG}}{\text{Å}^{-2}}\right)A_0(E_F)\ .$$

The FS information that one would really like to see would be the specification of the radius vector to any point that lies on the surface. Such information would constitute a complete geometric description

TABLE I. Experimental values for the dHvA frequencies (in MG) corresponding to extremal cross-sectional areas of the FS of Mo.

(001) Plane				($1\bar{1}0$) Plane				($1\bar{1}1$) Plane		
Label	Frequency this study	Other result[a]	Other result[b]	Label	Frequency this study	Other result[a]	Other result[b]	Label	Frequency this study	Other result[a]
	[010] direction				[001] direction					
β	5.19 ± 0.03	5.15	5.21	β	5.18 ± 0.03	5.17	5.33			
β	8.21 ± 0.04	7.92	8.23	β	8.25 ± 0.04	8.00	8.53			
σ	11.73 ± 0.05		11.78	σ	11.73 ± 0.05		12.30			
ρ	22.7 ± 0.1		23.0	ρ	22.7 ± 0.1		23.0			
ρ	29.9 ± 0.1		31.2	ρ	29.9 ± 0.1		31.1			
π	31.65 ± 0.1			π	31.63 ± 0.1					
ν	150.3 ± 0.6			ν	150.5 ± 0.5					
τ	231 ± 3			τ	232 ± 3					
	[110] direction				[110] direction				[110] direction	
β	5.12 ± 0.02		5.08	β	5.12 ± 0.02	5.03	4.95	β	5.10 ± 0.1	5.04
β	5.75 ± 0.02	5.70	5.76	β	5.76 ± 0.03	5.63	5.65	β	5.74 ± 0.1	5.75
ρ	25.1 ± 0.1		26.18	ρ	25.1 ± 0.1	24.2	25.76	ρ	25.0 ± 0.2	25.8
ρ	26.3 ± 0.1		27.96	ρ	26.3 ± 0.1		29.5	ρ	26.3 ± 0.2	25.8
σ	32.4 ± 0.1		32.25	σ	32.35 ± 0.1		30.8	σ	32.4 ± 0.2	
π	33.4 ± 0.15		34.0	π	33.4 ± 0.1			π	33.5 ± 0.2	
ρ	36.4 ± 0.1		40.1	ρ	36.45 ± 0.1		38.5	ρ	36.4 ± 0.2	
ω	•••			ω	76.0 ± 0.4			ω	75.6 ± 0.4	
ν	113.2 ± 0.4			ν	113.4 ± 0.4			ν	113.2 ± 0.4	
ϕ	158.0 ± 1.0			ϕ	158.7 ± 1.0			ϕ	158 ± 1.5	
					[112] direction				[121] direction	
				β	5.27 ± 0.03			β	5.28 ± 0.1	5.28
				β	6.04 ± 0.04			β	5.98 ± 0.1	5.97
				ρ	22.9 ± 0.1			ρ	23.0 ± 0.15	
				ρ	25.4 ± 0.1			ρ	25.2 ± 0.3	
				ρ	25.7 ± 0.1			ρ	26.1 ± 0.4	
				σ	26.3 ± 0.3			σ	27.6 ± 0.4	
				ρ	31.7 ± 0.1			ρ	31.7 ± 0.2	
				π	33.3 ± 0.1			π	33.6 ± 0.3	
				ξ	90.5 ± 0.4			ξ	89.0 ± 1.0	
				ν	109.5 ± 0.4			ν	108.2 ± 1.0	
					[111] direction					
				β	5.41 ± 0.03	5.37	5.45			
				ρ	24.0 ± 0.1		24.45			
				ρ	30.2 ± 0.1		30.9			
				σ	35.2 ± 0.2		36.4			
				π	35.4 ± 0.2					
				ξ	84.7 ± 0.4					
				ν	103.5 ± 0.4		108.6			

[a]See Ref. 14.

[b]See Ref. 15.

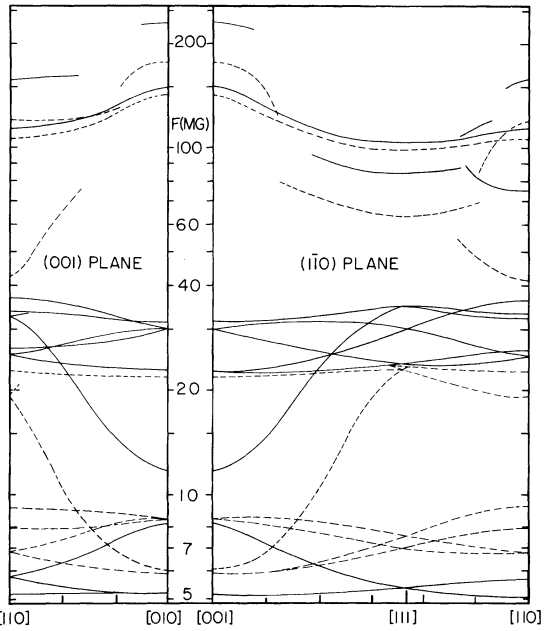

FIG. 9. Comparison of the dHvA frequencies of molybdenum and tungsten. The solid lines indicate molybdenum data from this study. The dashed lines indicate tungsten data from Ref. 20.

of the FS.

A quick qualitative comparison of the FS's of W and Mo can be made through the use of Figs. 8 and 9. Figure 8 is a drawing of a model FS for W. Figure 9 displays the Mo data from Fig. 2 as solid lines and the W data of Girvan *et al.*[20] as dashed lines. The band structures for these metals are similar, so qualitatively similar FS's are to be expected, except that *W* does not have lenses. The octahedra of both metals compare rather closely in size. The electron jack of Mo is quite a bit larger in body, ball, and neck dimensions than the one in W (note the logarithmic scale in Fig. 9). The lenses in Mo make a small contribution to the volume of the total electron FS pieces. The hole ellipsoids are much larger in Mo than in W, which is to be expected if the hole volume is to exactly compensate for the increased electron-jack volume and the volume due to the lenses. Remember that for each of these compensated metals the volumes of the electron FS pieces must equal the volumes of the hole FS pieces.

There are at least three ways of relating FS dimensions to the dHvA data: (i) An accurate band-structure calculation for Mo could be done from which FS radii could be obtained. The intersection of a plane with these radii could be integrated to determine the extremal areas one would expect to see in a dHvA experiment. The calculated areas could be compared with the experimental data and conclusions drawn about the accuracy of the band-structure calculation and about how consistent the data really are. (ii) The FS areas could be converted into FS radii by some inversion technique. The hole ellipsoids at *N* and the hole octahedron at *H* satisfy the requirements needed to invert the dHvA data to obtain FS radii by using computer programs[27] implementing the Mueller inversion scheme.[28] (iii) Simple or complex geometrical models could be devised at the appropriate symmetry point and used to predict experimental extremal cross-sectional areas. Sometimes the models can be revised until the desired accuracy of fit to the data is obtained.

An accurate band-structure calculation and predictions of the dHvA frequencies as a function of magnetic field direction were not available at the time this work was carried out. The numerical results of the APW calculations of Loucks[4] are questionable (see Sec. I). A new calculation by Iverson and Hodges,[5] presented in the article immediately following, is still not as accurate as the dHvA data from experiment, but this is true of all band calculations to date.

The inversion-scheme programs[27] will be used for the octahedra and the ellipsoids, but cannot be used on the lenses and jack. The difficulties encountered in applying the inversion scheme and the criteria for picking the number of coefficients to use in the expansion will be discussed shortly.

The eleven parameters of the fairly complex geometrical model for the W jack (see Ref. 20) were adjusted in an attempt to fit the Mo data. A program used to generate this model was obtained from Girvan.[29] While a few of the parameters could be successfully chosen to fit data coming from the body of the jack, no complete set was found that would come within even 5% of all the data points available at high-symmetry directions. The choosing of the parameters was done by hand, since the equation is highly nonlinear and the data are compared to integrals of the equation. This is not to say that a better set of eleven parameters does not exist, but the likelihood of easily finding this better set is considered small. Therefore, we shall attempt to use only very simple geometrical models to determine the dimensions of the jack and compare these with the results of other experiments.

A printing error exists in Appendix B of Ref. 27 containing the inversion programs. The Kubic harmonic expansion coefficients, necessary for use with the O_h-group inversion programs, have the leading two columns of each page missing. These columns should contain "sign" information about several of the numbers in the table. The first coefficient in the table also has the digit "1" dropped, which is necessary to obtain any results at all from programs using this information. A partial list of these coefficients in Ref. 30 was used in detecting this er-

ror and the complete list of correct values was later obtained from the program authors. One parameter, the cone angle, must be set at or near 90° rather than at 0°, which one might try as a first guess, since no "usual" value is quoted to guide the user of the programs.

The symmetry at N is such that eight frequency branches for the ellipsoids are obtained from data taken in only the (001) and $(1\bar{1}0)$ planes. The number of expansion coefficients uniquely determined by the data supplied to the inversion program is related not only to the number of data points, but also to the angular position at which the points are taken. Choosing to take data only in planes of high symmetry does place a limit on the number of coefficients which should be used for inversion. A general feeling for this limit develops as attempts are made to determine an increasingly larger number of coefficients. For the octahedron at H, the full cubic symmetry O_h applied. Here data taken in only the (001) and $(1\bar{1}0)$ planes cannot yield unique coefficients whose l value is greater than 18 (11 terms) (see Ref. 30). Including additional data from the $(1\bar{1}1)$ plane should increase this number of terms somewhat. The number of coefficients used in the final fit for each surface was determined by the lesser of the maximum number obtainable and the point at which addition of more coefficients would yield no further reduction in the standard deviation of the data from that predicted by the inversion scheme.

B. Hole Octahedron at H

The data relating to the octahedron, labeled ν in Fig. 2, from all three planes were used with the inversion scheme for the O_h symmetry group to obtain the FS radii for this piece of the total surface. The symmetry directions chosen for the $(1\bar{1}1)$ plane are those which are shown in Fig. 6.

As indicated in Sec. IV A, $l = 18$ with 11 coefficients is the highest unique fit for data from only the (001) and $(1\bar{1}0)$ planes. Using the radii determined from an $l = 18$ fit involving data from all three planes as a standard, the radii obtained for higher values of l were compared. None of the radii changed by more than ± 2% as the l value was increased. From the number of peaks and valleys in the curve for $l = 24$ it was assumed that the fit was probably sensitive to large changes in radii (surfaces of high curvature) only if those changes occur over angular intervals of approximately 10° or more.

The cross sections of the octahedron pieces of the FS for the (001), $(1\bar{1}0)$, $(1\bar{1}1)$, and $(1\bar{1}2)$ planes are shown in Figs. 10 and 11 for the $l = 24$ fit involving 19 coefficients, which are listed in Ref. 21. The $l = 24$ fit was chosen as the cutoff point where using additional coefficients would not further reduce the standard deviation of the input data from that predicted by the inversion scheme. In the $(1\bar{1}0)$ plane in Fig. 10, the RFSE caliper dimensions of Boiko *et al.*[17] were plotted directly, while the dimensions obtained by Cleveland[22] and Cleveland and Stanford[18] were multiplied by 1.05 before plotting. In the $(1\bar{1}0)$ plane the RFSE calipers for this piece of the FS are also the FS radii, except for angles near 50°, where the calipers would not be able to measure the slight dimple in the surface near these angles, and would, therefore, yield larger values than those of a plot of radii. At the [001] direction the RFSE measurement is probably more accurate than the radii indicated by the inversion scheme, since the surface has high curvature near this direction.

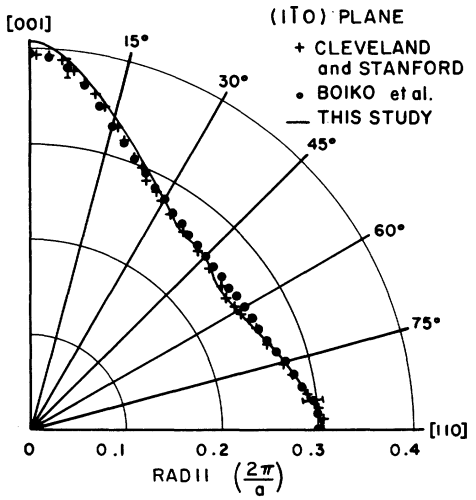

FIG. 10. Cross section of the hole octahedron FS at H for the $(1\bar{1}0)$ plane. The RFSE data of Boiko *et al.* (Ref. 17) have been plotted directly, while the RFSE data of Cleveland and Stanford (Ref. 18) have been multiplied by 1.05 before plotting.

Radii obtained from inversion of the dHvA data for the octahedron are tabulated for major symmetry direction in Table II. The volume calculated using the inversion coefficients in a suitable program from Ref. 27 was found to be 0.90 Å^{-3}. This compares with 0.90 Å^{-3} obtained by Boiko *et al.*[17] and 0.95 Å^{-3} estimated by Sparlin and Marcus.[15]

The octahedron radii found in the present experiment and the corresponding RFSE data of Boiko *et al.* agree to within the errors of the experiments. The plots of octahedron radii obtained from the present experiment are probably accurate to ± 1%, except near the [001] direction, where the errors are probably closer to ± 2%.

The RFSE octahedron dimensions reported by Cleveland and Stanford[18] for the (110) plane were integrated by computer and yielded an area of 0.98 ± 0.02 Å^{-2}. When these dimensions were in-

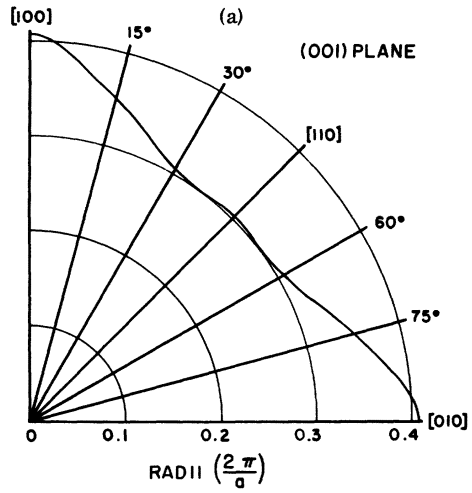

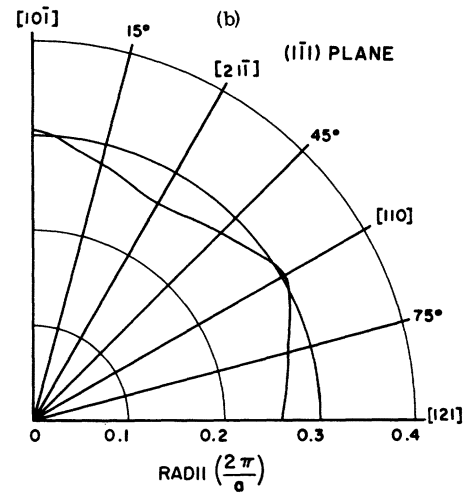

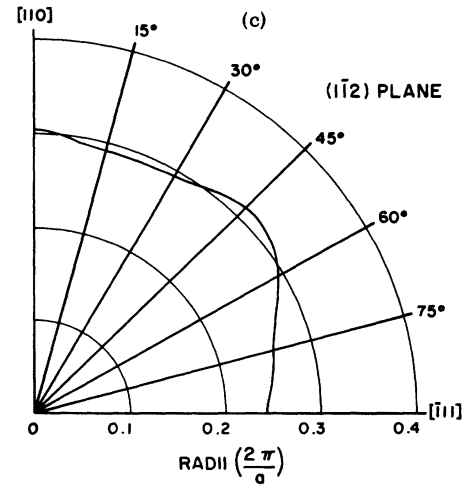

FIG. 11. Cross sections of the hole octahedron FS at H for the (001), (1$\bar{1}$1), and (1$\bar{1}$2) planes.

TABLE II. Radii for the hole octahedra in units of $2\pi/a$.

Direction	Inversion scheme radii	Others	
		Boiko *et al.*[a]	Cleveland and Stanford[b]
⟨100⟩	0.407	0.395	0.376
⟨110⟩	0.304	0.30	0.290
⟨111⟩	0.244	0.255	0.238
⟨112⟩	0.262	0.27	0.253

[a]See Ref. 17. [b]See Ref. 18.

creased by 1.05, the resulting area matched the 1.083 ± 0.01-Å^{-2} cross-sectional area for this direction obtained in the present experiment. From the manner in which these RFSE dimensions, plotted in Fig. 10 after being multiplied by 1.05, compare with this study and with the RFSE calipers of Boiko *et al.*, it would appear that the work of Cleveland and Stanford was subject to a systematic error of 5%. In Ref. 18 they are aware that their results do not agree with those of other investigators and have considered in detail the sources of error in their experiment (an RFSE investigation employing extensive frequency studies). Their investigation was thorough and does not contain obvious weaknesses. Using samples cut from the same single-crystal rod, experimental data are presented which disagree with their work, but we must conclude as they did concerning their work that "the reasons for the disagreement are at present unknown."[18]

C. Hole Ellipsoids at N

All of the data labeled ρ in Fig. 2 come from the hole ellipsoids at N. These frequency branches, four from the (001) plane and four from the (1$\bar{1}$0) plane, were used as input in the inversion scheme for the $V_h(D_{2h})$ symmetry group along with the two frequency branches from the (1$\bar{1}$1) plane which are the most insensitive to small errors in sample orientation. These latter two were the branches connecting the 31.7-MG frequency at the ⟨112⟩ directions with either the 36.4- or 25.0-MG frequencies at the [110] direction as shown in Fig. 6 with the choice of symmetry directions as indicated on that figure.

There are 12 symmetry points N in the Brillouin zone, and generally six frequency contributions to the dHvA effect for an arbitrary magnetic field direction from a FS piece appropriately situated at equivalent pairs of these points, but one must concentrate on a single point N in order to obtain results from the inversion scheme. The problem can be viewed as one in which an ellipsoid with axes a, b, and c along three coordinate directions

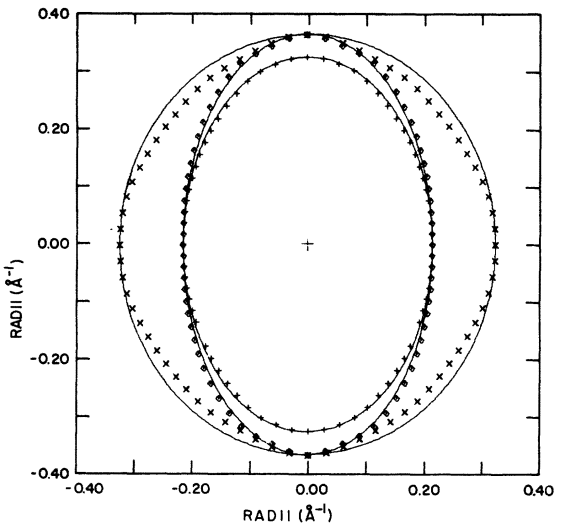

FIG. 12. Cross sections of the hole ellipsoid FS at N for the planes containing the three semiaxes. These directions are $N\Gamma$, NH, and NP.

k_x, k_y, and k_z is placed with point N at (0,0,0) and the four frequency branches from the (001) plane are thought to come from four separate planes of observation on the single ellipsoid, and similarly for any other experimental plane of observation. As a check on the data assignments made, computed dHvA data generated from a perfect ellipsoid were fed into the inversion scheme and checked with the areas calculated by the inversion scheme. The appropriate choice of spherical mapping coefficients[31] could also be determined from these ideal data.

The three principal cross sections for the ellipsoid pieces situated at symmetry points N are shown in Fig. 12 with different plotting symbols for each of the cross sections. The solid curves are plots of perfect ellipses having major and minor axes identical to those obtained from the inversion scheme for the $l=16$ fit involving 45 coefficients. These 45 coefficients along with the two spherical mapping parameters are listed in Ref. 21. The $l=16$ fit was the highest-order fit that could be obtained and was chosen because the standard deviation of the input data from that predicted by the inversion scheme was lower than that of any other fit obtained for a lower l value.

Values for the three semiaxes of the ellipsoids at N as found with the inversion scheme are listed in Table III. Since it is impossible to decide upon the assignment of semiaxes to the NH and $N\Gamma$ directions from the dHvA data, it is assumed that the shortest semiaxis is along NH, which is consistent with the FS calculations for Mo by Loucks.[4] The volume calculated using the inversion coefficients in a suitable program from Ref. 27 was found to be 0.614 Å^{-3} for 6 hole ellipsoids. This compares with 0.61 Å^{-3} obtained by Boiko *et al.*[17] and 0.71 Å^{-3} obtained by Sparlin and Marcus.[15]

The column labeled "estimated from three areas" in Table III contains semiaxes as calculated from the frequencies (and corresponding areas) which exhibit the condition that $dF/d\theta=0$ at ⟨110⟩ or ⟨100⟩ directions. These three frequencies correspond to the extremal cross sections πab, πbc, πac for a perfect ellipsoid at N. The semiaxes a, b, and c calculated in this manner can only be as good as the approximation that the actual surface is a perfect ellipsoid. As can be seen from Fig. 12, the largest cross section has some places which are flatter than the perfect ellipse with same semiaxes, so semiaxes estimated in this manner would be expected to differ from those determined by the inversion scheme. The inversion scheme radii for this surface should be accurate to about 1%.

D. Electron Lenses at Δ

Data related to the electron lenses at symmetry point Δ along ΓH in the Brillouin zone cannot be inverted by Mueller's inversion scheme, since this point does not possess inversion symmetry. The physical significance of this fact is that dHvA experiments cannot provide enough information about this surface to specify a *unique* surface consistent with the required C_{4v} symmetry. If an additional condition is imposed that the surface has a mirror plane whose normal is parallel to ΓH, the point has now been given the D_{4h} symmetry, which satisfies inversion theorem requirements, and enables use of the Mueller inversion scheme or use of a geometrical model with the additional symmetry. However, when this additional re-

TABLE III. Values in Å^{-1} for the semiaxes of the hole ellipsoids at N.

Direction	Inversion scheme radii	Estimated from three areas	Other Investigations: Boiko *et al.*[a]	Cleveland and Stanford[b]	Sparlin and Marcus[c]
NP	0.365	0.358	0.38	0.35	0.39±0.01
$N\Gamma$	0.325	0.310	0.29	0.32	0.30±0.01
NH	0.216	0.223	0.22	0.20	0.23±0.01

[a]See Ref. 17. [b]See Ref. 18. [c]See Ref. 15.

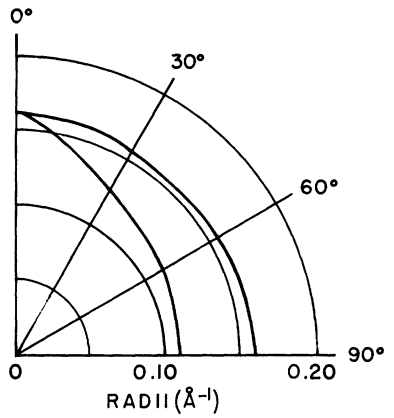

FIG. 13. Cross sections of the electron lens FS at Δ assuming a higher D_{4h} symmetry. For the nearly circular cross section, the plane has normal direction ΓH, and 0° and 90° are parallel to ⟨100⟩ directions.

quirement is imposed to obtain a unique fit to the data, the surface obtained is only a possible substitute for the actual surface. It is possible, but rather unlikely, that the real FS exhibits this mirror symmetry.

The condition of fourfold symmetry in a plane whose normal is parallel to ΓH for the point Δ and the almost zero slope of the lowest frequency branch of the experimental data for the (001) plane (see Fig. 3) can be combined to suggest that the lenses are very nearly circular with radius r in a cross section whose normal is parallel to ΓH. The dHvA data about the lens's cross section having a dimension d along ΓH as one axis and the lens's radius r as the other axis are not sufficient to specify the distance α between the center of the plane of the circular cross section and the center of the ΓH dimension. It can be shown by simple geometrical arguments that two different cross sections with identical values for r and cross-sectional areas, but differing in values of α and d, should be distinguishable because of differing caliper dimensions for the same angle of observation.

This effect is probably only noticeable as a 4–5% difference in caliper dimensions, unless the lenses are highly asymmetrical. In other words, the RFSE might be able to distinguish between symmetrical and asymmetrical models which could both agree with the dHvA results. However, unless the RFSE data are very accurate, probably better than 1%, the amount of asymmetry along the ΓH direction could not be determined quantitatively. Such accuracy cannot be expected from RFSE orbits yielding small caliper dimensions, since these resonances are detected at low magnetic field strengths where $\omega_c\tau$ is low and the RFSE line shapes are broad. Another result of the geometrical arguments is that while the distance α can vary quite widely, the ΓH dimension for the lens remains reasonably constant, as does the volume of the FS.

For the above reasons, the five frequency branches for the (001) and $(1\bar{1}0)$ planes shown in Fig. 3 were used as input to the inversion scheme for the D_{4h} symmetry group. As with the ellipsoids discussed in Sec. IV C, one lens was picked and placed at the origin of an inversion k space and all of the data were used as if they had been taken from five different planes of observation. The program was checked with perfect ellipsoids of revolution and the spherical mapping parameter was also determined from these ideal data.

The two principal cross sections for the lens pieces situated at symmetry points Δ are shown in Fig. 13, subject to the additional symmetry requirement necessary for inversion of the data. The results obtained from the inversion scheme for the $l=16$ fit involving 25 coefficients, which are listed along with the spherical mapping parameter GAMMA in Ref. 21, came from the highest-order fit that could be obtained.

Values obtained with this fit for the radii of the electron lenses at Δ for the approximately circular cross section are 0.162 $Å^{-1}$ for a direction parallel to ⟨100⟩, 0.155 $Å^{-1}$ for a direction parallel to ⟨110⟩, and a total ΓH dimension of 0.222 $Å^{-1}$ in the direction perpendicular to the circular cross section. The volume calculated using the inversion coefficients in a suitable program from Ref. 27 was found to be 0.057 $Å^{-3}$ for 6 lenses. This compares with a volume of 0.060 $Å^{-3}$ obtained by Leaver and Myers.[16]

E. Electron Jack at Γ

An accurate model for the electron-jack surface is the most difficult to extract from the dHvA data of extremal cross-sectional areas. The data cannot be inverted by using the Mueller inversion scheme because some radius vectors to points on the surface are multivalued. There is no way to accurately determine the position of the center of the ball connected to the body portion of the jack. In Sec. IV B it has been shown that the RFSE data of Boiko *et al.*[17] agree quite closely with the radii obtained from inversion of the octahedron dHvA data. Their RFSE data will be used to supply some valuable jack radii, but only at those angles where there is good reason to believe that the caliper dimensions obtained in the RFSE experiment are actually radii. The claim made by Boiko *et al.*[17] that "upon rotation of the magnetic field relative to the crystallographic directions in the (110) plane, the lines of the experimental points from the extremal orbits of the electron 'jack' will give directly the section of this surface with the (110)

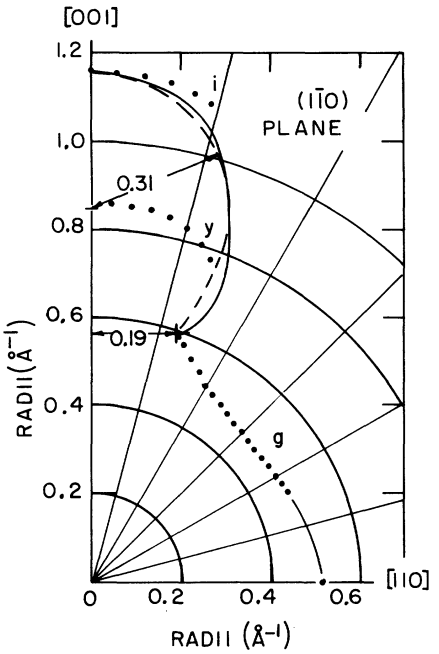

FIG. 14. (1$\bar{1}$0) plane cross section for the electron-jack FS at Γ. The ● and ○ data points and their labels are RFSE results of Boiko *et al.* (Ref. 17). The + data point at 19° from [001] and the solid line construction are described in the text.

plane" is not true for the entire jack cross section in this plane. In particular, the line "i" of the data of Boiko *et al.*,[17] shown as plotted points in Fig. 14, can be coincident with the actual radius vector only at the [001] direction. At any other angular position for this line, the RFSE measures caliper dimensions, and must be interpreted as such. It is easy to fall into the trap of equating caliper dimensions with radii for surfaces whose curvature and symmetry does not allow such a statement to be true. In general, for all but very simple FS shapes extreme care should be exercised when equating RFSE calipers with FS radii.

In the following paragraphs the rationale for the particular (1$\bar{1}$0) and (001) cross sections for the electron jack as shown in Figs. 14 and 15 will be presented. First some facts obtained directly from the data should be noted. In Sec. IV D the electron lenses were seen to be very nearly circular. Since the lenses lie in the neck portions of the jack and the lens and neck cross sections are comparable in size, it seems reasonable to assume that the necks are also very nearly circular. From the value of 11.7 MG at the ⟨100⟩ directions for the neck orbit labeled σ in Fig. 2, a radius of 0.19 Å^{-1} for a circular neck cross section is obtained. For the (1$\bar{1}$0) plane, the ball orbit labeled π in Fig. 2 yields values of 31.63 MG at [001], 33.4 MG at [110], and 35.4 MG at [111]. The neck cross section is 32.4 MG at [110]. Assuming a rather spherical shape for the ball, and a circular cross section for the [001] direction, a radius of 0.310 Å^{-1} is obtained for the ball. The angles at which the body orbit labeled ξ in Fig. 2 disappears in the (1$\bar{1}$0) plane can help to define the neck dimensions. At a magnetic field direction of $19 \pm \frac{1}{2}°$ from [110] the neck interferes with the completion of the body orbit, and the orbit is no longer possible. This corresponds to the loss of RFSE signals at $21 \pm 2°$ from a ⟨100⟩ direction reported by Cleveland and Stanford,[18] and at $21 \pm 3°$ from a ⟨100⟩ direction reported by Boiko *et al.*[17] Note that RFSE data are plotted as caliper dimensions for given directions and are obtained with fields applied perpendicular to the given direction and to the plane of the sample. At a magnetic field direction of $27 \pm 2°$ from [100], the orbit around the body changes into an orbit which encompasses all four balls. A loss of RFSE signals at $29 \pm 2°$ from a ⟨110⟩ direction was reported by Cleveland and Stanford, and at $24 \pm 3°$ from a ⟨110⟩ direction by Boiko *et al.*

In Fig. 14 for the (1$\bar{1}$0) plane the RFSE calipers of Boiko *et al.* at [001] and [110] are assumed to be radii, as well as those arising from the body of the jack, labeled *g*. The radii are 1.16 Å^{-1} at [001] and 0.52 Å^{-1} at [110]. An additional data point + for the body at 19° from [001] was extrapolated as indicated by our data. This point also defines the neck radius at 0.19 Å^{-1} for a circular neck cross

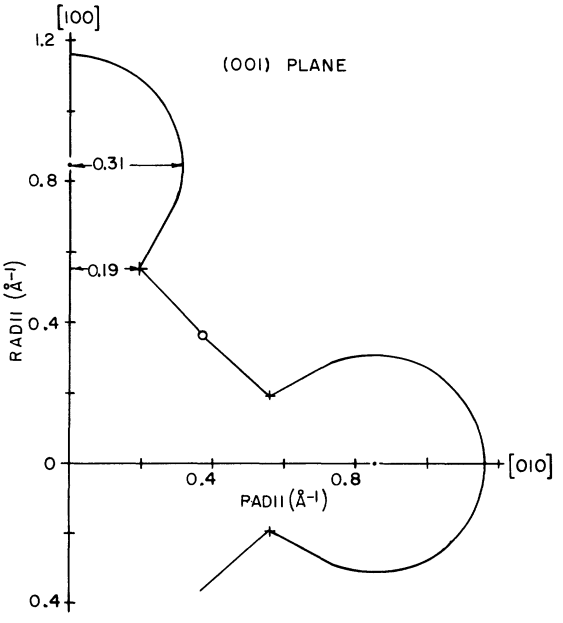

FIG. 15. (001) plane cross section for the electron-jack FS at Γ. The ○ is a data point from Ref. 17. The + data points and the solid line construction are described in the text.

section. A completely spherical ball is shown dashed in along with a straight line to connect the neck to the ball, and a gently curved solid line is drawn connecting the body data with the data point at [110].

A spherical ball with circular neck and ball cross sections at ⟨100⟩ directions was assumed for the ball and neck drawn in Fig. 15 for the (001) plane. The RFSE data point at [110] was included and a slightly curved line was drawn to connect the necks with this point. The body is slightly concave at [110] in this plane, a fact which agrees with the observation of two neck frequencies near 32.4 MG at small angles away from [110] in the (001) plane, as shown in Figs. 2 and 4. The area computed for the model (001) plane is 2.19 $Å^{-2}$ which compares very favorably with 2.21 $Å^{-2}$ for the dHvA experimental area.

An area integration of the $(1\bar{1}0)$ plane as it has been constructed thus far yields 1.45 $Å^{-2}$ to be compared with the dHvA experimental value of 1.51 $Å^{-2}$. The value for this area can be improved and the model corrected so that both a minimum (neck) and maximum (ball) cross section is observable at the [110] direction where the experimental data shows values of 32.4 and 33.4 MG by drawing the additional (solid) lines for the ball. The new area for the $(1\bar{1}0)$ plane is 1.49 $Å^{-2}$. An integration to check the neck and ball cross sections at [110] quantitatively is impossible to do accurately without a complete analytical description of the surface to be analyzed.

It is not possible to carry this simple geometrical model further or make additional comparisons with the experimental data since the integrations of cross-sectional areas which do not contain the center of symmetry for the figure and/or whose normal is not a direction of high symmetry are possible only with an analytical model suitable for a computer. The assumption about fairly spherical balls is also likely to break down somewhat as one adjusts the model for a more accurate fit. As mentioned in Sec. IV A, the analytical approach was tried with no better results than those presented above.

V. CONCLUSIONS

The dHvA data for molybdenum which have been presented are accurate to within 1% in frequency or 1° in angle, whichever is the larger error, for the magnetic field rotated in the $(1\bar{1}0)$, (001), and $(1\bar{1}1)$ crystallographic planes. Two samples, cut from the same single-crystal rod as the sample used in the RFSE work of Cleveland and Stanford,[18] were used to obtain the dHvA data. These data were shown to be consistent in frequency and angular determination at the appropriate major symmetry directions for the above mentioned planes. The data were inverted through the use of the Mueller inversion theorem,[28] when possible, to obtain FS radii, and a simple geometrical model was developed for the electron jack. The FS radii for the $(1\bar{1}0)$ plane cross section for the hole octahedron obtained from the dHvA data were shown to be consistent with the RFSE caliper dimensions obtained by Boiko *et al.*[17] for the same plane. The geometrical model for the electron-jack cross section is consistent with the RFSE caliper dimension at [001]. Since the inversion-radii data for the octahedron are most subject to error at [001], the determination by Boiko *et al.* of the RFSE caliper dimensions, which are radii at [001], is believed to be correct. These RFSE dimensions for the ⟨100⟩ direction are 1.16 $Å^{-1}$ for the jack and 0.79 $Å^{-1}$ for the octahedron with the ΓH dimension as 1.999 $Å^{-1}$, so the gap between the jack and octahedral FS pieces is estimated as 2.5% of the ΓH dimension, thus resolving the discrepancies existing in current RFSE data.

The model presented for the electron jack could probably be improved by further calculations on a complicated analytical model. An accurate FS model based on band-structure calculations for molybdenum would be more desirable, but such calculations are not yet precise enough for agreement with experiment. The recent energy band calculations of Iverson and Hodges appear in the following article.[5]

ACKNOWLEDGMENTS

It is a pleasure to acknowledge the digital equipment design by Dr. P. T. Panousis and valuable discussions with Professor A. V. Gold, Professor R. A. Phillips, and Professor D. L. Pursey.

---

*Based on work submitted to Iowa State University in partial fulfillment of requirements for the Ph.D. degree. Present address: Computation Center, Iowa State University, Ames, Ia. 50010.

[1]W. M. Lomer, Proc. Phys. Soc. Lond. **80**, 489 (1962).
[2]J. H. Wood, Phys. Rev. **126**, 517 (1962).
[3]W. M. Lomer, Proc. Phys. Soc. Lond. **84**, 317 (1964).
[4]T. L. Loucks, Phys. Rev. **139**, A1181 (1965).
[5]R. J. Iverson and L. Hodges, following paper, Phys. Rev. B **8**, 1429 (1973).
[6]E. Fawcett, Phys. Rev. **128**, 154 (1962).
[7]E. Fawcett and W. A. Reed, Phys. Rev. **134**, A723 (1964).
[8]N. E. Alekseevskii, V. S. Egorov, G. E. Karstens, and B. N. Kazak, Zh. Eksp. Teor. Fiz. **43**, 731 (1962) [Sov. Phys.-JETP **16**, 519 (1963)].
[9]E. Fawcett and D. Griffiths, J. Phys. Chem. Solids **23**, 1631 (1962).
[10]C. K. Jones and J. A. Rayne, in *Proceedings of the Ninth*

International Conference on Low Temperature Physics, edited by J. G. Daunt, D. V. Edwards, and M. Yaqub (Plenum, New York, 1965), p. 790.
[11]P. A. Bezuglyi, S. E. Zhevago, and V. I. Denisenko, Zh. Eksp. Teor. Fiz. **49**, 1457 (1965) [Sov. Phys.-JETP **22**, 1002 (1966)].
[12]R. Herrmann, Phys. Status Solidi **25**, 661 (1968).
[13]G. B. Brandt and J. A. Rayne, Phys. Lett. **3**, 148 (1962).
[14]G. B. Brandt and J. A. Rayne, Phys. Rev. **132**, 1945 (1963).
[15]D. M. Sparlin and J. A. Marcus, Phys. Rev. **144**, 484 (1965).
[16]G. Leaver and A. Myers, Philos. Mag. **19**, 465 (1969).
[17]V. V. Boiko, V. A. Gasparov, and I. G. Gverdtsiteli, Zh. Eksp. Teor. Fiz. **56**, 489 (1969) [Sov. Phys.-JETP **29**, 267 (1969)].
[18]J. R. Cleveland and J. L. Stanford, Phys. Rev. B **4**, 311 (1971).
[19]L. F. Mattheiss, Phys. Rev. **139**, A1893 (1965).
[20]R. F. Girvan, A. V. Gold, and R. A. Phillips, J. Phys. Chem. Solids **29**, 1485 (1968).
[21]J. A. Hoekstra, Ph.D. thesis (Iowa State University, 1972) (unpublished).
[22]J. R. Cleveland, Ph.D. thesis (Iowa State University, 1970) (unpublished).
[23]C. P. Bean, R. W. DeBlois, and L. B. Nesbitt, J. Appl. Phys. **30**, 1976 (1959).
[24]P. T. Panousis, Ph.D. thesis (Iowa State University, 1967) (unpublished).
[25]P. T. Panousis and A. V. Gold, Rev. Sci. Instrum. **40**, 120 (1969).
[26]W. J. O'Sullivan and J. E. Schirber, Cryogenics **7**, 118 (1967).
[27]R. L. Aurbach, J. B. Ketterson, F. M. Mueller, and L. R. Windmiller, in *The Inversion of de Haas–van Alphen Data: I. Closed Surfaces with Inversion Symmetry* (Argonne Natl. Lab. Report No. ANL-7659, Argonne, Ill., 1970). Available from Natl. Tech. Info. Service, U. S. Dept. of Commerce, Springfield, Va. 22151.
[28]F. M. Mueller, Phys. Rev. **148**, 636 (1966).
[29]R. F. Girvan (private communication).
[30]F. M. Mueller and M. G. Priestly, Phys. Rev. **148**, 638 (1966).
[31]J. B. Ketterson and L. R. Windmiller, Phys. Rev. B **1**, 463 (1970).

PHYSICAL REVIEW B VOLUME 8, NUMBER 4 15 AUGUST 1973

Molybdenum: Band Structure, Fermi Surface, and Spin-Orbit Interaction

R. J. Iverson* and L. Hodges
Ames Laboratory-USAEC and Department of Physics, Iowa State University, Ames, Iowa 50010
(Received 26 December 1972)

The nonrelativistic energy bands of bcc Mo are calculated by the renormalized-atom method and the Fermi surface is obtained using an interpolated band structure. The de Haas–van Alphen data for the neck orbit of the electron jack and the electron lens are used to derive, for the crystal, a spin-orbit parameter of 0.0075 Ry, approximately equal to the atomic spin-orbit parameter.

I. INTRODUCTION

The experimental data relating to the Fermi surface (FS) of bcc Mo have been reviewed by Hoekstra and Stanford in the preceding paper.[1] The FS of Mo has four sheets qualitatively similar to those of the minority-spin electrons in iron[2]: I, hole pockets ("ellipsoids") centered at the points N in the Brillouin zone; II, a hole octahedron centered at the point H; III, an electron "jack" centered at the point Γ; IV, electron lenses centered on the Δ symmetry lines.

In the absence of spin-orbit coupling the octahedron and jack would contact each other on the Δ symmetry line and each lens would contact a "neck" of the electron jack just off the Δ axis. The spin-orbit interaction in Mo produces separations between these pairs of surfaces.

The separation between the octahedron and the jack is of particular interest because reported experimental estimates of its value differ by more than the reported experimental errors. The radio-frequency-size-effect (RFSE) measurements of Boiko *et al.*[3] give a separation of $(2.5\pm2)\%$ of the ΓH dimension $2\pi/a$ while those of Cleveland and Stanford[4,5] give $(7.5\pm2)\%$.[5] The latter value is estimated to require a spin-orbit parameter of 0.03 Ry,[4] which is 4 times the atomic spin-orbit parameter of 0.0074 Ry calculated by Herman and Skillman.[6] The de Haas–van Alphen (dHvA) data of Hoekstra and Stanford[1] are consistent with the smaller value of the separation, that of Boiko *et al.*, but not consistent with that of Cleveland and Stanford.

The rest of this paper discusses the interpolated band structure of Mo, the resulting FS, and the value of the spin-orbit parameter obtained from a fit to the experimental dHvA data. The results indicate that the separation along the Δ axis between the octahedron and the jack is only about 1.2% of $2\pi/a$.

II. BAND STRUCTURE

Previous nonrelativistic band-structure calculations for Mo have been reported by Loucks[7] and Petroff and Viswanathan.[8] We originally intended

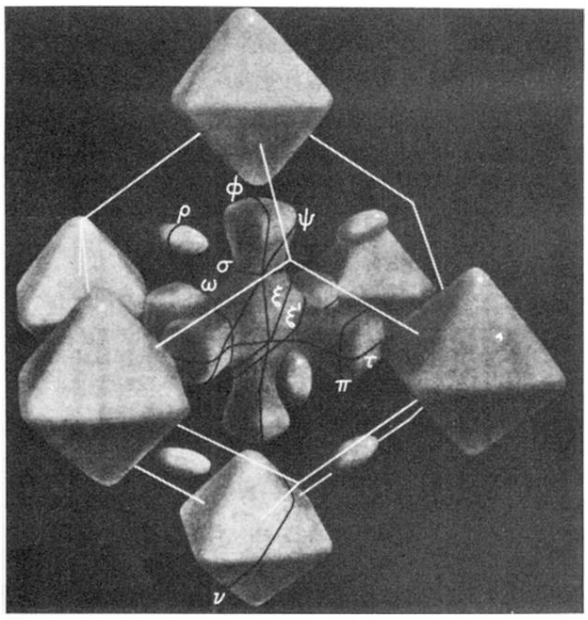

FIG. 8. Drawing of a model FS for tungsten, whose FS is similar to that for molybdenum. Some extremal orbits expected to give rise to a dHvA effect are shown as black lines. The Brillouin zone is indicated by white lines. Differences between the FS of molybdenum and tungsten are discussed in Sec. IV A. Figure reproduced from Ref. 20.